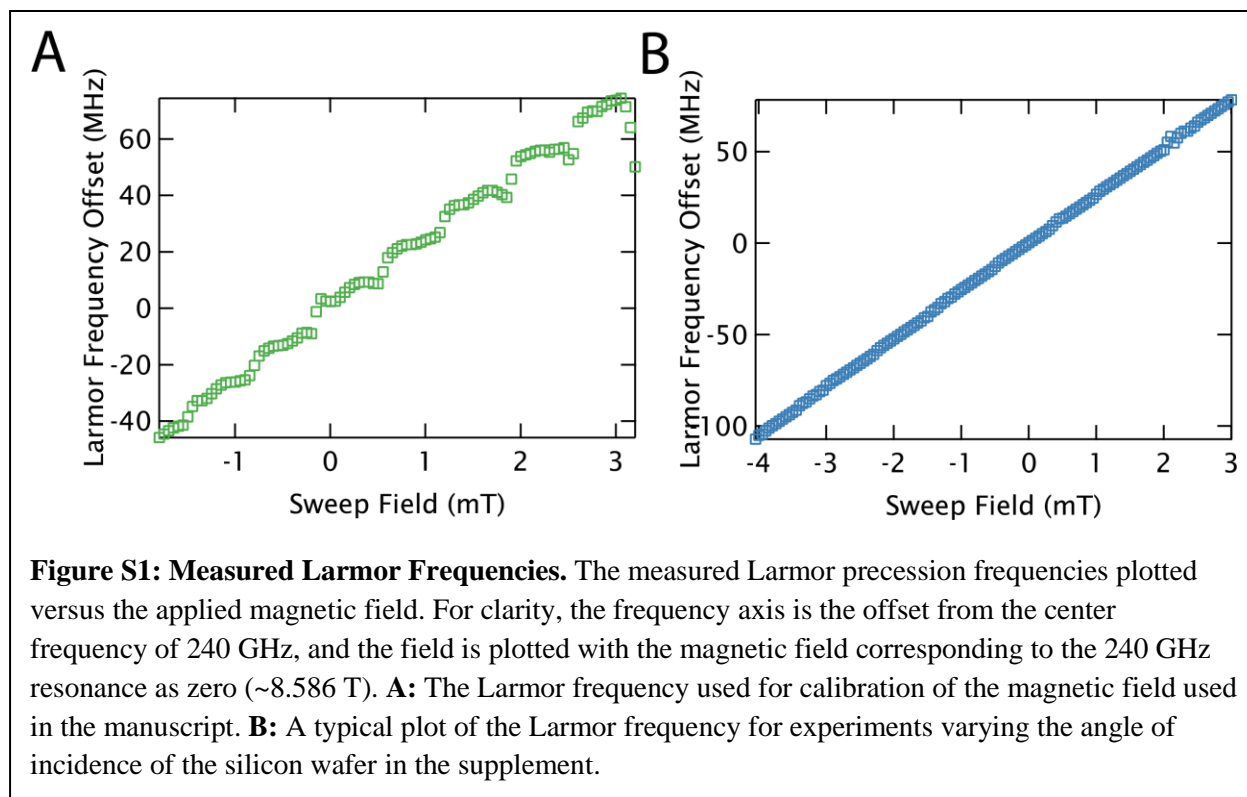


## Supplemental Material

### 1) Data Collection for the Measurement of Relative Phase between Two Pulses

Here some details are provided of the measurements of the transverse magnetization as a function of offset frequency. It covers the use of the Cavity Dump Coupler (CDC), the data collection and processing, and the determination of Larmor frequency from field. The CDC was used as a Q-switch to suddenly lower the quality factor of the FEL cavity at the same time that the second sliced pulse was ended.<sup>1</sup> This prevents lasing after the end of the second pulse in order to eliminate scattered light and leakage from appearing during the FID. An additional, though in this case unnecessary, result is that the CDC offers a roughly two-fold increase in  $B_1$  amplitude for the second pulse. As the magnetic field was stepped, the sweep coil was allowed to briefly settle before the magnitude of the Fast Fourier Transform (FFT) of the FID was recorded. As the resonance moves when the magnet field is swept, the area was always measured in a window of roughly  $\pm 100$  MHz about the center frequency of 500 MHz (the IF frequency) to ensure the entire signal was included at every field point. 3 scans were taken at each field to determine an average value and standard deviation for each field/frequency point. Occasional misfires of the FEL cause missed pulses, where the FEL does not lase. This caused large disruptions to the data, and so a filter was applied to eliminate scans where no FID was visible above the noise. This filter acted during data collection, and so did not change the number of scans for each point (if a result was discarded, another scan was taken). This filtering acted only to screen out the clear cases when the FEL failed to fire as the cutoff criterion was always far smaller than the weakest measured FID, ensuring it did not skew the results.

The measurement of field from the superconducting magnet is based on a calibration of the



applied current, and shows appreciable drift over days. This was accounted for differently in the data presented in the manuscript and in the supplement. For the measurements presented in the main manuscript, during one field sweep each FID was saved (in addition to the integrated, magnitude FFT area) and later processed to create an accurate map from the measured magnetic field to the Larmor frequency of the BDPA sample. This map was created using a linear fit, and the variation in Larmor frequency due to the sample magnetization was ignored as it was small. A plot showing the Larmor frequency as a function of the swept field, which was used for this calibration, is shown in Fig. S1A and shows the small deviations from linearity mentioned above. The effect is discussed further in section 2 of this supplement. For subsequent scans only the integrated FFT area was recorded, and the measured magnetic field was used to determine the Larmor frequency based on the previously generated map. Although this was sufficient to observe clear oscillations, there were some fluctuations that likely emerged from small field drifts. For the high-precision measurements of the phase in section 4 of the supplement, the Larmor frequency was measured for each experiment in order to avoid any drifts in the magnetic field during the day. Interestingly, for these measurements, the relation between the Larmor frequency and magnetic field was found to be entirely linear, and showed no effects from the magnetization of the sample. A representative data set of showing the Larmor frequency as a function of the swept field, is shown in Fig. S1B.

## 2) Effect of Magnetization on Precession Frequency

The high concentration of spins in the BDPA grain results in a high-field magnetization large enough to appreciably affect the precession frequency of the spins (though the strength of the shift can vary from sample to sample due to a strong dependence on sample geometry). As a result, the precession frequency is modified slightly depending on the rotation of the magnetization vector. As noted, this can be seen as small oscillations in the measurement of the Larmor precession frequency vs. magnetic field that was used for calibration in the main text. However these oscillations were much smaller than the range of frequencies that was swept through. Further, the Larmor frequency of the FID is not the actual Larmor frequency during the pulse sequence. This makes it difficult to compensate for this small effect. The absence of an observed effect in the data in the supplement likely emerges as the result of either a differing sample geometry of the grain, or differing tip angles (in the case of smaller tip angles due to less FEL power, the magnetization is modified less during the pulse sequence). However, we have also observed cases where this effect can be more disruptive, most notably in observation of Rabi oscillations, which will be investigated in future work.

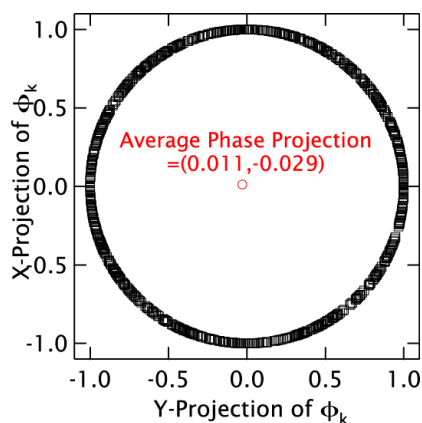


**Figure S2: Random Phase of the FEL.**

Shows the x- and y- projections of the pulse phase ( $\phi_k$ ). As the reference phase is not locked to the FEL, the relative phase samples the unit circle effectively randomly. The center shows the average x- and y- projections approaches 0.

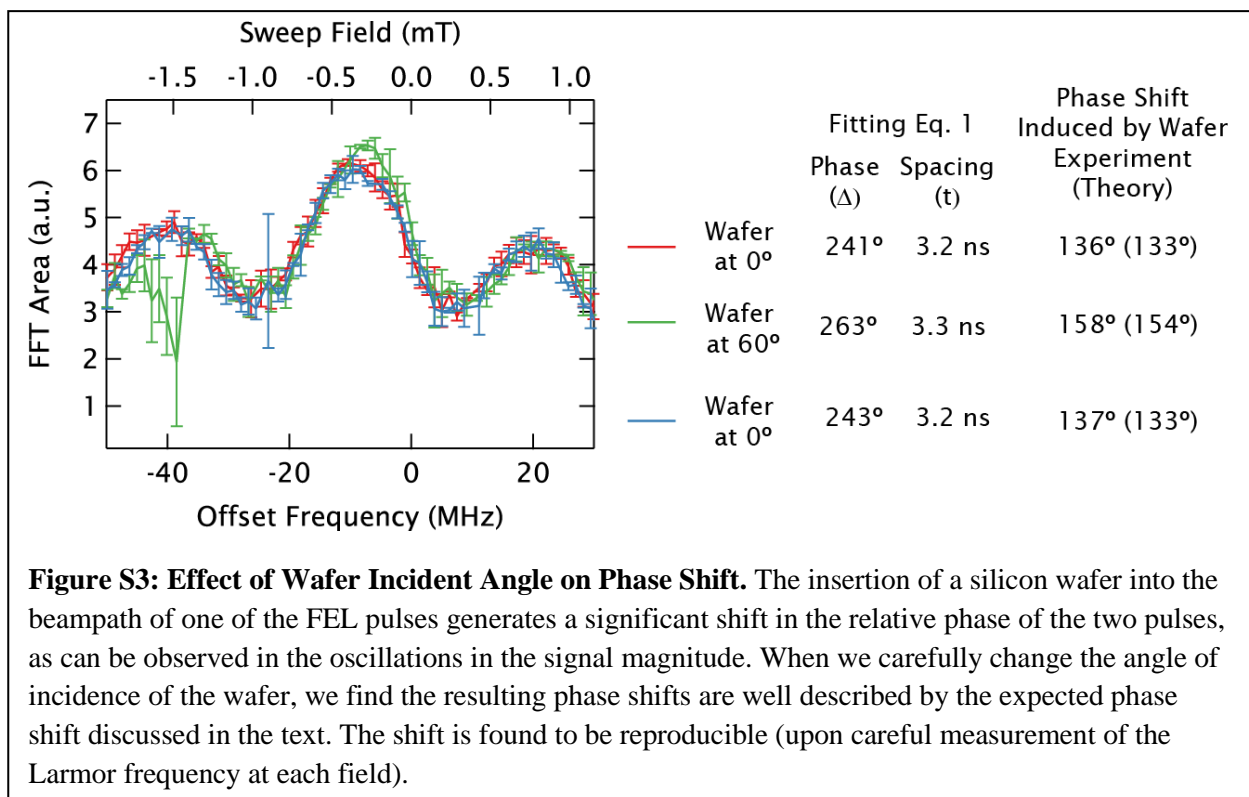
### 3) Random Phase of the FEL Relative to the Detector

Fig. S2 shows the real (x) and imaginary (y) parts of the relative phase factors  $\exp(i\Delta\phi_k)$  of the 890 pulses compared to the first of those pulses. The relative phase was measured following the procedure in the manuscript. The points roughly cover the unit circle evenly and the average phase factor ( $= \frac{1}{N_{tr}} (\sum_k \exp(i\Delta\phi_k))$ ) approaches zero, confirming that the phase is random (as expected) with respect to the unlocked reference.

### 4) Tuning Phase with Angle of Incidence of a Dielectric Wafer

A silicon wafer, inserted into one pulse's path changes the pathlength as the wafer's index of refraction is substantially different than air, and so the 240 GHz pulse acquires a substantially different phase across the wafer. This results in a change to the relative phase of the two pulses, which manifests itself as a phase shift in the oscillation of the area of the absolute value of the FFT of the FID as a function of offset frequency. The phase shift caused by the insertion of a dielectric material is determined by the index of refraction of the material, its thickness, as well as the angle that it's inserted at. Therefore, by tuning the angle of the wafer, we can tune the phase shift that is achieved. The phase acquired across a dielectric material can be written as<sup>2</sup>

$$\Phi(n, \theta_i) = \frac{n_s \omega d \cos(\theta_r[n, \theta_i])}{c}$$

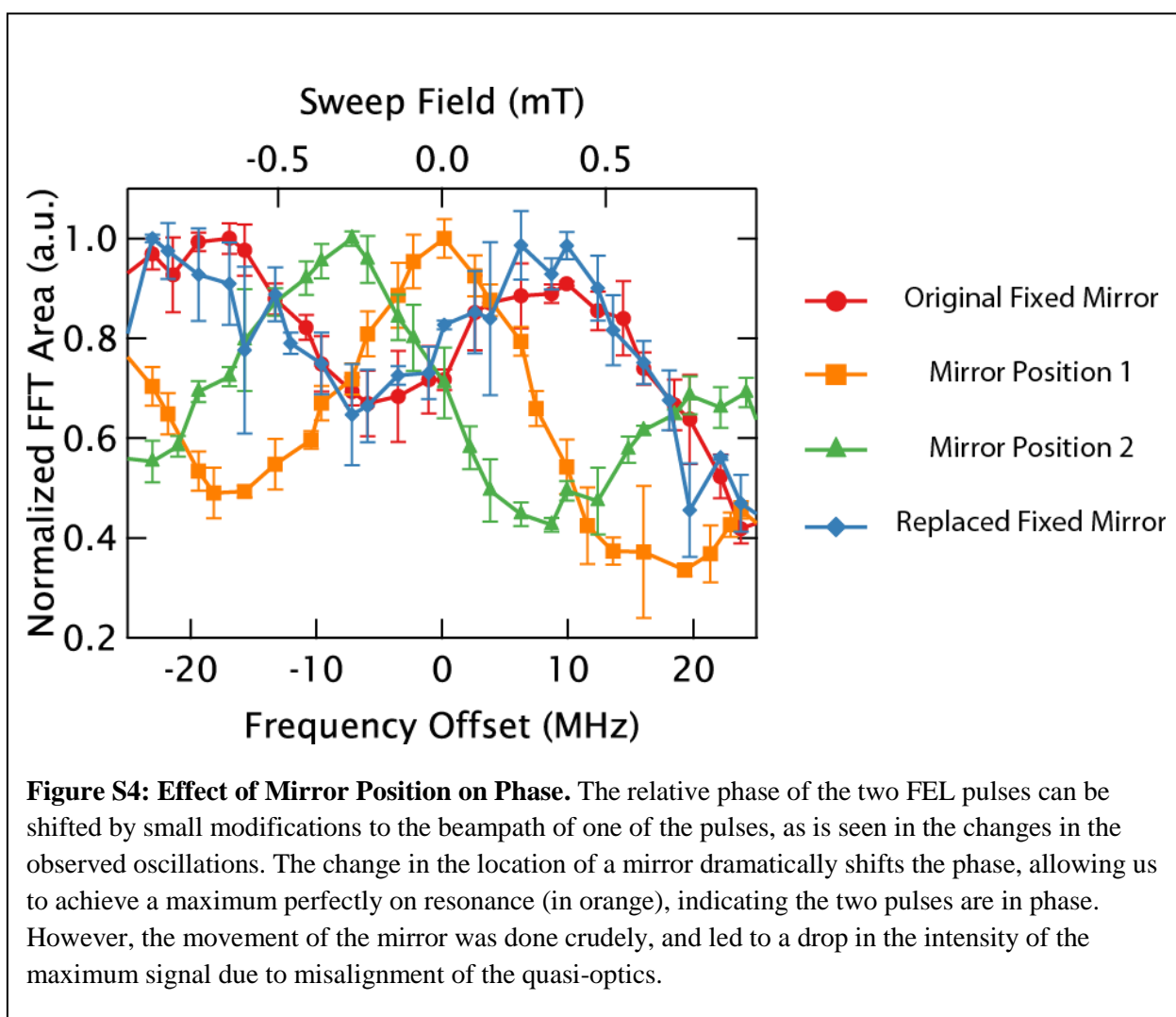


**Figure S3: Effect of Wafer Incident Angle on Phase Shift.** The insertion of a silicon wafer into the beampath of one of the FEL pulses generates a significant shift in the relative phase of the two pulses, as can be observed in the oscillations in the signal magnitude. When we carefully change the angle of incidence of the wafer, we find the resulting phase shifts are well described by the expected phase shift discussed in the text. The shift is found to be reproducible (upon careful measurement of the Larmor frequency at each field).

where  $n$  is the index of the dielectric material ( $n = n_s \approx 3.42$  for silicon),  $\omega$  is the frequency,  $d$  is the thickness of the material,  $c$  is the speed of light, and  $\theta_r$  is the propagation angle of the light in the material.  $\theta_r$  can be calculated from Snell's law:  $\theta_r = \arcsin(\frac{n_a}{n} \sin(\theta_i))$ , where  $n_a \approx 1$  is the index of refraction of air, and  $\theta_i$  is the angle of incidence. Thus, the expected change in phase can be written as the difference in phase acquired across the silicon wafer as opposed to the air that is displaced, i.e.

$$\Phi(n_s, \theta_i) - \Phi(n_a, \theta_i) = \begin{cases} 133^\circ, & \theta_i = 0^\circ \\ 154^\circ, & \theta_i = 60^\circ \end{cases}, \text{ based on our best estimate of } d \sim 191 \mu\text{m}.$$

In order to measure the phase of the oscillations as accurately, a set of measurements was carried out where the Larmor frequency of the spins was explicitly measured at each field point (rather than being calibrated from the measured field). The difference in the shift can be observed experimentally as shown in Fig. S3, but is small (here a  $\sim 20^\circ$  shift corresponds to  $< 2$  MHz). Further, when the angle of incidence is returned to the initial setting of  $0^\circ$ , the trace returns to its original location. We can use the analytic expression for the oscillations (manuscript Eq. (1)) to determine the phase shift by fitting the data, and the results are also shown in Fig. S3. The shifts are found to agree well with the phase shifts expected from the calculations. The calculated shifts are consistently  $\sim 3\text{-}4^\circ$  less than measured, indicating some systematic error in the measurement, or calculation of the relative phase. These could emerge from the effects of the FEL pulse having a Gaussian spatial profile when passing through the wafer, from errors in the fitting to the numerical expression or from error in determination of the thickness of the wafer. Nonetheless, the effect of rotating the wafer from a  $0$  to a  $60^\circ$  incident angle, is found experimentally to be  $21\text{-}22^\circ$ , which agrees almost perfectly with the calculated value of  $21^\circ$ . Further, the choice of incident angle is currently only limited by the radial size of the wafer relative to the 240 GHz beam waist, meaning that incident angles out to  $\sim 75^\circ$  can be used, which should allow modification of the phase by  $> 30^\circ$



##### 5) Tuning Phase through Small Modifications of the Beam Path

A physical change in the path length of one pulse will also introduce a change in the relative phase of the two pulses. However, the short wavelength of light at 240 GHz ( $\lambda \approx 1.25$  mm), means that changes on the order of 10's of  $\mu\text{m}$  can lead to appreciable changes in phase ( $10^\circ$  corresponds to  $35 \mu\text{m}$ ). Thus, very small changes to the quasi-optical pathway should allow fine tuning of the relative phases of the two pulses. This is demonstrated experimentally in Fig. S4, where the phase of the FID intensity oscillations is shown to shift for small changes in location of the mirror. We show that the phase of the oscillations can be shifted so that the maximum is located near to the zero-frequency offset as shown in orange, indicating that the two pulses are in phase. The current setup did not include a micro-positioner and so the changes were done by physically shifting the mirror mount, which prevents accurate tuning. Fig. S4 shows the normalized signal for clarity, as the tuning of the wafer position affected up to a  $\sim 25\%$  drop in maximum intensity, which emerges from incorrectly changing the rotation of the mirror to correct for the change in position. However, inclusion of a mirror designed to be moved over  $\sim 1$  mm, would allow precise tuning of the relative phase of the pulses and will make it easier to correctly modify the rotation of the mirror to account for the translation.

### 6) Fit Values for Offset Oscillations

These are the values used when fitting the equation

$$M_{tr} = A\sqrt{1 - (\cos(\alpha)\cos(\beta) - \cos(\omega t - \Delta)\sin(\alpha)\sin(\beta))^2}$$

to the offset-frequency dependent oscillations. Here A is an arbitrary amplitude parameter,  $\alpha$  and  $\beta$  are the tip angles of the first and second pulse,  $\omega$  is the offset frequency, and  $\Delta$  is the relative phase of the two pulses.

#### i) Varying Pulse Lengths (Figures 7 and 8)

Nominal Spacing (ns)	Fit Spacing t (ns)	Fit Relative Phase $\Delta$ (°)	Fit Amplitude A (a.u.)	Fit $\alpha$ (°)	Fit $\beta$ (°)
40	42.1	-137	158	15.8	9.4
45	46.7	-128	161	15.8	9.4
55	56.8	-130	137	15.8	9.4

#### ii) Inserting Wafers (Figure 9)

Nominal Spacing (ns)	Wafer /Angle (°)	Fit Spacing t (ns)	Fit Relative Phase $\Delta$ (°)	Fit Amplitude A (a.u.)	Fit $\alpha$ (°)	Fit $\beta$ (°)
40	No	42.1	-137	158	15.8	9.4
40	Yes/134	42.1	24	136	15.8	9.4
40	No	42.3	-116	150	15.8	9.4

#### iii) Tuning Wafer Angle (Supplemental Figure 2)

Nominal Spacing (ns)	Wafer Angle (°)	Fit Spacing t (ns)	Fit Relative Phase $\Delta$ (°)	Fit Amplitude A (a.u.)	Fit $\alpha$ (°)	Fit $\beta$ (°)
30 (Not Plotted)	No Wafer	31.1	105	2385	7.5	4.9
30	0	31.9	241	2249	7.5	4.9
30	60	32.6	263	2174	7.5	4.9
30	0	32.1	243	2225	7.5	4.9

### Supplemental References

1. S. Takahashi, G. Ramian and M. S. Sherwin, *Applied Physics Letters*, 2009, **95**, 234102.
2. J. Jackson, *Classical Electrodynamics Third Edition*, Wiley1998.